NANO LETTERS

Letter

pubs.acs.org/NanoLett

Topological Surface Transport Properties of Single-Crystalline SnTe Nanowire

Muhammad Safdar,† Qisheng Wang,† Misbah Mirza, Zhenxing Wang, Kai Xu, and Jun He*

National Center for Nanoscience and Technology, Beijing 100190, China

Supporting Information

ABSTRACT: SnTe has attracted worldwide interest since its theoretical predication as topological crystalline insulator. Because of promising applications of one-dimensional topological insulator in nanoscale electronics and spintronics device, it is very important to realize the observation of topological surface states in one-dimensional SnTe. In this work, for the first time we successfully synthesized high-quality single crystalline SnTe nanowire via gold-catalyst chemical vapor deposition method. Systematical investigation of Aharonov-Bohm and Shubnikov-de Haas oscillations in single SnTe nanowire prove the existence of Dirac electrons. Further analysis of temperature-dependent Shubnikov-de Haas oscillations gives valuable information of cyclotron mass, mean-free path, and mobility of Dirac electrons in SnTe nanowire. Our study provides the experimental groundwork for research in low-dimensional topological crystalline insulator materials and paves the way for the application of SnTe nanowire in nanoelectronics and spintronics device.

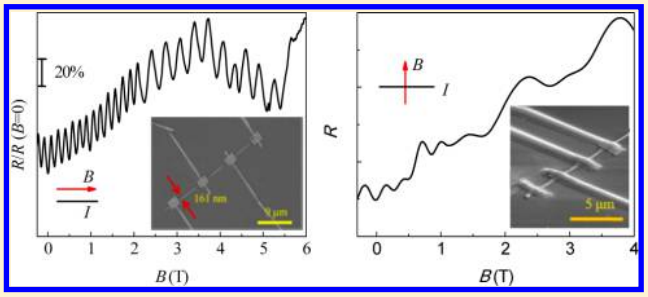

KEYWORDS: *Single-crystalline SnTe nanowires, topological crystalline insulators, Aharonov-Bohm interference, Shubnikov-de Haas oscillations*

Topological insulators (TIs), an unusual quantum state of matter, are characterized by a gapless metallic surface state and insulating bulk gap.[1] On the surface of TIs, the electron spin is locked perpendicular to the momentum, which make the surface state of TIs immune to any time reversal perturbations such as nonmagnetic impurities and crystal defects.[2−4] These unique properties make TIs promising applications in novel spintronics and low-dissipation quantum computation.[5,6] In addition, TIs provides the basis of materials for realization of unique quantum mechanical effect such as quantum anomalous hall effect[7] and Majorana fermions.[5]

The discovery of three-dimensional (3D) TIs protected by time-reversal symmetry[8] such as Bi_2Te_3, Sb_2Te_3, and Bi_2Se_3 has simulated the search of new topological insulator protected by other symmetries. For example, topological crystalline insulators (TCIs),[9] a new topological state, are found to be protected by crystal symmetry. Among various materials, tin telluride (SnTe) with a rocksalt structure shows special mirror symmetry in face-centered cubic Brillouin zone. It has been predicted as the first distinctive type of TCIs where conductive surface states are expected on the highly symmetrical crystal surface of SnTe such as {001}, {110} and {111}.[10] Since the discovery of SnTe as remarkable TCIs, it has attracted worldwide interest and opens the gateway to the theoretical and experimental research of TCIs. Significantly, SnTe is a simple stoichiometric compound compared with other TCIs such as $Pb_{1-x}Sn_xTe$,[11] which make it easier to be synthesized. Recently, Tanaka[12] et al. experimentally confirmed the existence of a metallic Dirac-cone surface state on the (001) surface of SnTe bulk crystals by angle-resolved photoemission spectra. However, very few magneto-transport measurements of TCIs SnTe,[13] a straightforward way to probe the surface topological states, have been reported presumably due to the dominant transport of bulk carriers from crystal defects and thermal excitations.[3]

Compared with bulk counterparts, nanostructure TIs materials are highly competitive system for investigating the surface topological nature due to their large surface-to-volume ratio,[14−16] leading to an enhancement of contribution of topological surface carriers. In addition, nanostructures of TIs play a vital role for fundamental investigation of materials such as exotic surface states and spintronics applications.[17−19] As a result, it is of particular important to study the surface electronic state of TCI SnTe nanostructures by magneto-transport experiment. However, to the best of our knowledge, there is no experiment evidence showing the topological crystalline insulator nature of SnTe nanostructure. This may be due to the challenges in synthesis of high quality single crystalline low-dimensional SnTe nanosturctures.

Here, we report for the first time the synthesis of highly single crystalline SnTe nanowire via gold-catalyst chemical vapor deposition (CVD) and the observation of topological

Received: July 30, 2013
Revised: October 22, 2013
Published: October 31, 2013

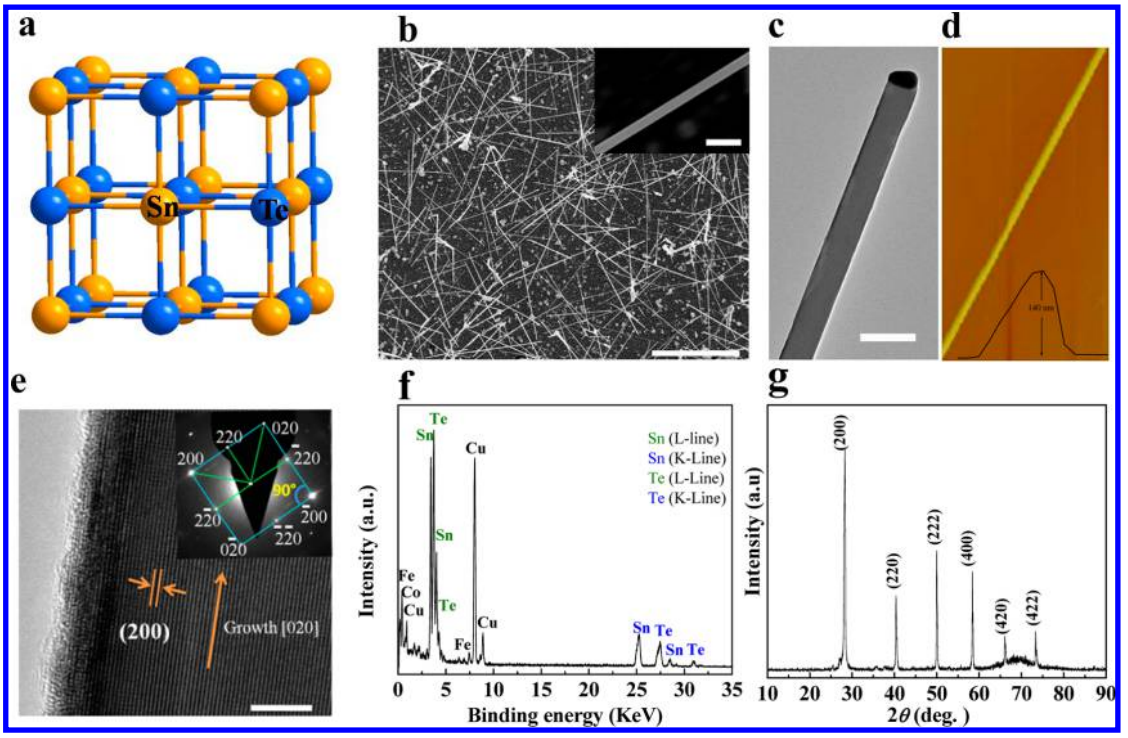

Figure 1. Microscopy measurement of SnTe nanowires. (a) Schematic view depictions of the cubic crystal structure of SnTe. (b) SEM images of SnTe nanowires, inset is a high-magnification image. The scale bar in (b) is 10 μm and inset is 200 nm. (c) TEM images of single SnTe nanowire with gold particle at the top. The scale bar in (c) is 200 nm. (d) AFM image of single SnTe nanowire, inset shows cross-section shape of SnTe nanowire. (e) HRTEM images and SAED pattern (inset) of single crystalline SnTe nanowire, three white spots (000), (220), and (020), shaded by the tip, were artificially added. The scale bar in (d) is 5 nm. (f) EDS of obtained SnTe nanowires. (g) XRD pattern of as prepared SnTe nanowires.

surface states in SnTe nanowire by quantum oscillation measurement. The quantum transport measurement of SnTe nanowire shows well distinguished Aharonov-Bohm (AB) interference and Shubnikov-de Haas (SdH) oscillations. Deep analysis of AB oscillation shows the existence of both h/e and $h/2e$ quantum oscillations, giving the evidence of topological surface states. Investigation of SdH oscillations indicates the existence of π Berry phase, which demonstrates that quantum oscillation arises from two-dimensional Dirac fermions. Valuable parameters of topological surface states such as cyclotron mass, mean-free path, and mobility of Dirac electrons in SnTe nanowire are also estimated by analyzing the temperature-dependent SdH oscillation.

SnTe nanowires used in this work were synthesized in a horizontal tube furnace via CVD method. Well-aligned and dense nanowires were obtained on Au-coated Si substrate with SnTe powder used as an evaporation source.[20] More details of the growth process and characterization are described in the Supporting Information. SnTe has a cubic crystal structure with space group $Fm3m$ as described in Figure 1a. Schematic diagram of electronic structure of SnTe (001) surface is also provided in Supporting Information Figure S1.[21] The typical low-magnification scanning electron microscopy (SEM) image shown in Figure 1b clearly illustrates the synthesized samples are composed of dense nanowires with about 10 μm long. The nanowires density of this substrate with deposition temperature of 500 °C is estimated to be 1.7 × 10^9/cm^2 (Supporting Information Figure S2a). High-magnification SEM image (Figure 1b inset) reveals the synthesized nanowires are about 59 nm in diameter. The diameters of nanowires in this substrate primarily distribute in 50−99 nm (75%), the diameters of other nanowires are in the range of 100−199 nm (25%), the average diameter in this substrate is 98 nm (Supporting Information Figure S2b). Transmission electron microscopy (TEM) image of nanowire in Figure 1c exposes the presence of gold nanoparticle at the top of nanowire, suggesting the vapor−liquid−solid (VLS) growth mechanism. Magnified-TEM in Supporting Information Figure S3 shows top gold nanoparticle connected perfectly with SnTe nanowire. High-quality AFM images of several typical SnTe nanowires display cross-section shape of nanowire is mainly triangle (Figure 1d and Supporting Information Figure S4). Detailed structural characterizations using high-resolution TEM (HRTEM) image in Figure 1e demonstrate that SnTe nanowires are in well-defined single crystal cubic phase with the lattice fringes of 0.315 nm, corresponding to (200) plane. Figure 1e also signifies the surface of nanowire is smooth and has not been oxidized. It is found that nanowire growth is along [020] direction. The corresponding selected area electron diffraction (SAED) pattern (inset of Figure 1e) indicates excellent single crystalline of SnTe. The crystal planes (002), (020), and (022) suggest that the synthesized SnTe belongs to cubic crystal system (JCPDS 08-0487). Energy dispersive X-ray spectroscopy (EDS) study in Figure 1f indicates that nanowires have perfect stoichiometric ratio of Sn to Te 1:1, the peaks of copper, iron, and cobalt comes from copper grid. Moreover, no extra peaks are present in the X-ray diffraction pattern (Figure 1g) of nanowires, which further confirms the crystalline nature and pure cubic phase of SnTe.

AB oscillation originates from quantum interference of two partial electron waves after completing closed trajectories which encircle certain magnetic flux. In our study, we fabricated standard four terminal device for the observation of AB oscillation. Details of device fabrication and transport measure-

dx.doi.org/10.1021/nl402841x | Nano Lett. 2013, 13, 5344−5349

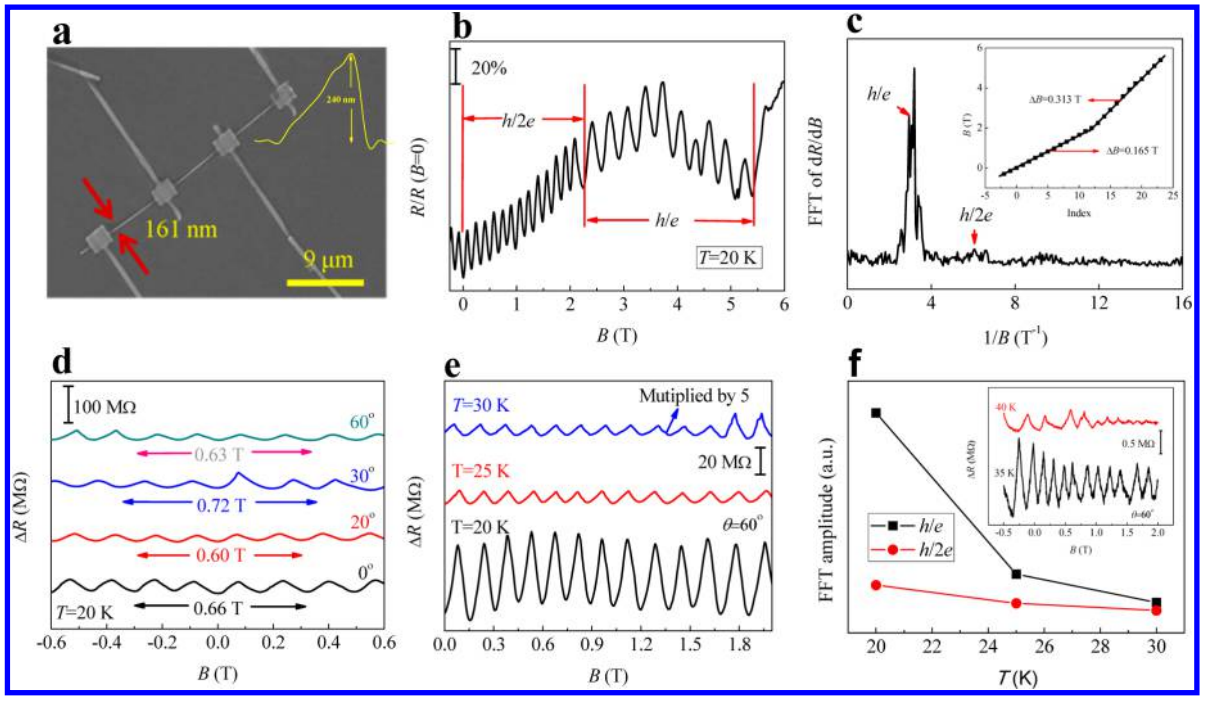

Figure 2. AB oscillation of topological surface states in SnTe nanowire. (a) SEM image of four terminal device of SnTe nanowire with bottom width of 161 nm and height of 240 nm. Inset: AFM indicates the triangular cross section of SnTe nanowire. (b) Normalized MR with applied parallel magnetic field at 20 K. (c) FFT of the derivate dR/dB indicates two oscillation frequency h/e and $h/2e$. Inset: magnetic field positions of oscillation minima versus oscillation index gives oscillation period of 0.165 and 0.313 T. (d) Angle-dependent MR oscillation, the colored arrows indicate the four oscillation periods. (e) Temperature dependence of MR oscillation, the period of MR oscillation keeps rather constant 0.15 T at 20, 25, and 30 K. The angle between magnetic field and nanowire keeps 60°. To clearly display the periodicity of MR at 30 K, the MR is amplified by 5 times. (f) Temperature-dependent FFT amplitude of derivate dR/dB for both h/e and $h/2e$ oscillation. Inset: aperiodic MR oscillation at 35 and 40 K indicates surface states are suppressed by bulk carriers at high temperature.

ments are given in Supporting Information. From Figure 2a, we can see that the nanowire has near triangle shape with a bottom width w of 161 nm and height h (Figure 2a inset) of 240 nm, giving the cross-section area $S = 1/2wh = 19\,320$ nm^2. When applied a parallel magnetic field along the length of the nanowire at temperature 20 K, the pronounced reproducible oscillation is observed as shown in Figure 2b. A downward sharp cusp at zero magnetic field shows the weak antilocalization effect, resulting from strong spin−orbit coupling of Dirac electrons as occurred in other TIs.[14,15,22] A fast Fourier transform (FFT) of magnetoresistance (MR) derivative dR/dB in Figure 2c displays prominent oscillation frequency of h/e. In addition, an oscillation frequency of $h/2e$, known as the Altshuler−Aronov−Spival (AAS) effect, has also been observed. The AAS effect, arising from quantum interference of two interfering electron wave encircling the magnetic flux once, has been realized in carbon nanotubes,[23] metal rings[24] and TIs.[15,25] Figure 2b shows AAS effect with the period of 0.165 T (Figure 2c inset) dominates at low magnetic field $0 < B < 2$ T, proving the existence of weak (anti)localization with strong enough disorder.[26] Conductance oscillation is expected to have a period of $h/2e$ in strong enough disorder topological insulator due to weak antilocalization away from the Dirac point.[26] SnTe is an intrinsic heavy p-type doped semiconductor due to large amount of Sn vacancies at finite temperature.[27,28] Thus SnTe nanowire achieved from our work is strongly enough disordered because a large quantity of holes likely exists inside SnTe nanowire. So AAS effect is intensely anticipated to occur in SnTe single crystalline nanowire at least in low magnetic field. However, with the increase of field $2\text{ T} < B < 5.3$ T, AB effect becomes dominant with reproducible oscillation period of 0.313 T (Figure 2c inset). However, the perfect periodicity deteriorates when magnetic field reaches up to 5.3 T, which may due to aperiodic oscillation from bulk carriers at high magnetic field. The obvious magnetoresistance oscillation has also observed at 2 and 10 K as shown in Supporting Information Figure S5. The period of AAS interference at 2 K is 0.169 T which is very close to the results measured at 20 K.

It is noted that, for the h/e AB effect period ΔB of AB oscillation is related to the magnetic flux quantum $\Phi_0 = h/e$ by $\Delta B = \Phi_0/S$, where S is the cross-sectional area of nanowire, h is the planck's constant, and e is the electron charge. Thus cross-sectional area of 13340 nm^2 can be deduced from AB oscillation which is slightly smaller than the estimated cross-sectional area of 19 320 nm^2 by SEM and atomic force microscopy (AFM). It is known that metallic surface states of SnTe exist on those surfaces with high symmetry such as {001}, {110}, and {111}. Thus it is not like topological insulator Bi_2Se_3 nanoribbon[15] or Ag_2Te nanowire[22] that spin-locked Dirac electron wave travels along the perimeter of nanoribbon or nanowire which forms a loop encircling magnetic flux. Loops formed by two interfering partial wave are confined to high-symmetry crystal surface inside SnTe nanowire, leading to the differences between cross-section area of 13 340 nm^2 obtained from the oscillation and that of 19 320 nm^2 estimated from results of SEM and AFM. This can be further verified through angle-dependent AB oscillation. As shown in Figure 2d, with an increase of angle θ between the nanowire and magnetic field, the oscillation period does not increase following $\Delta B(\theta) = \Delta B(0)/\cos(\theta)$. Here, ΔR represents the MR after subtraction of smooth background. If we suppose the normal direction of

dx.doi.org/10.1021/nl402841x | Nano Lett. 2013, 13, 5344−5349

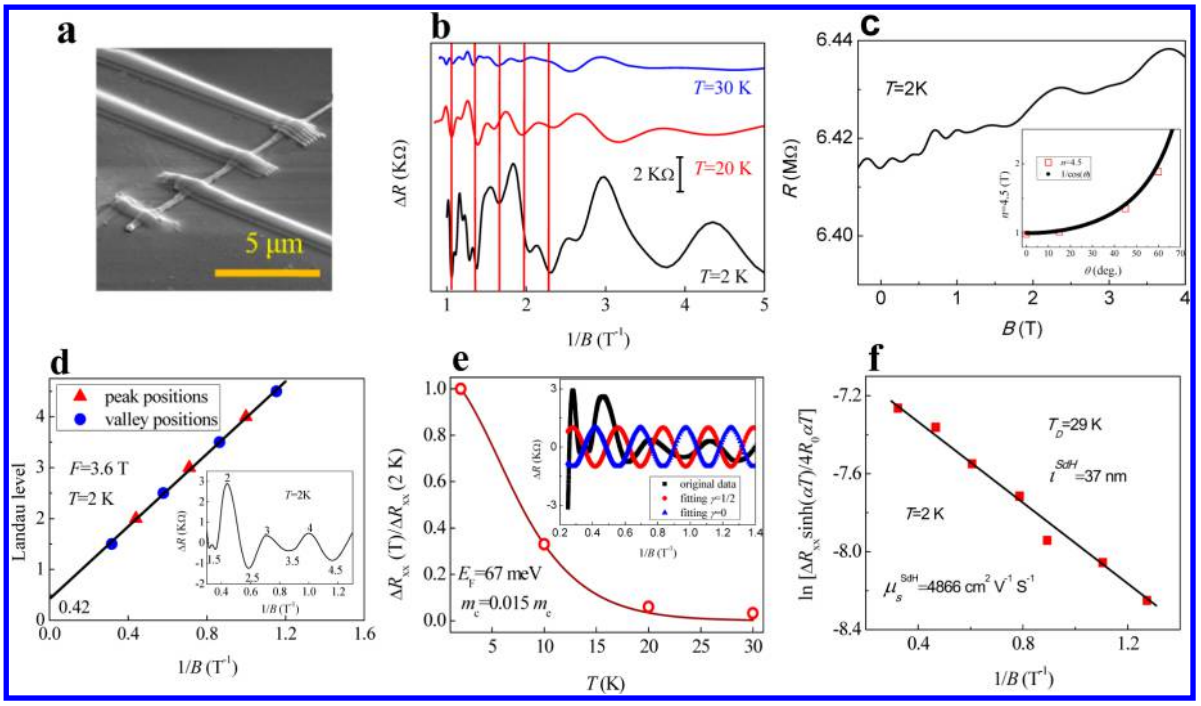

Figure 3. SdH oscillation of surface states in SnTe nanowire. (a) A 45°-titled-view SEM image of four terminal device of SnTe nanowire with width of 190 nm. (b) MR after subtraction of smooth background versus $1/B$ at 2, 20, and 30 K, red solid line shows the oscillation period remains constant with the increase of temperature. (c) MR versus B at 2 K with the magnetic field applied up to 4 T. Inset: valley position of $n = 4.5$ against tilted angle θ, the data are consistent with the fitting plot of $1/\cos(\theta)$. (d) LL fan diagram constructed from MR oscillation. Inset: integer and semi-integer show the Landau level of peak and valley, respectively. (e) Temperature dependence of SdH oscillation amplitude at $B = 0.72$ T, giving cyclotron mass 0.015 m_e. Inset: comparison of resistance oscillation at 2 K with well-known SdH oscillation of ideal 2D Dirac electrons ($\gamma = 1/2$) and regular electrons ($\gamma = 0$). (f) Dingle plot of SdH oscillation at 2 K, indicating the Dingle temperature T_D is 29 K, mean-free path l^{SdH} is 33 nm and mobility of surface electron μ_s^{SdH} is 4866 cm^2 V^{-1} s^{-1}.

loops is parallel to the growth direction of SnTe nanowire, loops may form on high-symmetry crystal surface (002), (200), $(00\bar{2})$ and $(\bar{2}00)$ faces since the growth direction of SnTe nanowire is [020]. However, loops are also possibly present on the other high-symmetry crystal surface. The normal directions of these loops are no longer parallel to growth direction of SnTe nanowire. Consequently, even if angle increases to 60°, the oscillations still keep strong because normal direction of some loops may go along the direction of magnetic field.

Next, we discuss the information of AB oscillation by analyzing temperature-dependent MR oscillation as shown in Figure 2e. Although the temperature increases to 30 K, the ΔR still shows markedly periodicity at the whole applied magnetic field region. As pointed out previously, the AAS effect is predominant at low field. In addition, AAS effect is more robust than AB effect against temperature because AAS effect is caused by quantum interference of two time-reversal turns of surface state moving. Thus periodic oscillation keeps powerful even at relative high temperature. This can be further proved via comparing temperature-dependent FFT amplitude of derivate dR/dB at each temperature as displayed in Figure 2f. FFT amplitude of oscillation h/e decreases sharply with increase of temperature while FFT amplitude of oscillation $h/2e$ almost keeps the same. However, as the temperature reaches up to 35 K, as shown in the inset of Figure 2f, the perfect periodicity of MR oscillation gradually deteriorates with increase of magnetic field. Even more, no period has been observed at 40 K (Figure 2f inset), which is likely due to that dominant transport of bulk carriers smears oscillations of topological surface states at high temperature. All of these behaviors suggest the existence of Dirac electrons in SnTe nanowire. This can be directly proved by the following results of SdH oscillations.

As a powerful tool, SdH oscillations are widely used to prove the existence of surface topological states.[29] The relatively large width of 190 nm (Figure 3a) of SnTe nanowire make SdH oscillations measurement available due to that approximate rectangle shape provides large top and bottom surface as displayed in the AFM (Supporting Information Figure S6). Magneto-transport measurements were carried out at low temperature with magnetic field B aligned perpendicular to the SnTe nanowire. Figure 3b presents the plots of ΔR versus $1/B$ at temperature of 2, 20, and 30 K, respectively. Strong oscillations can be observed at each temperature. The oscillation amplitude increases with the increase of magnetic field, demonstrating the SdH oscillations. Red lines in Figure 3b show the periodic oscillation of MR versus $1/B$ at each temperature. Figure 3c signifies a large positive MR effect of SnTe nanowire with no saturation as B increases to 4 T. An obvious downward cusp in MR at low field reflects the existence of weak antilocalization effect expected in the TIs due to the strong spin−orbit interaction and the helicity of the surface states.[14,15,30,31] Plot of MR versus $1/B$ (Supporting Information Figure S7) exhibits perfect periodic oscillation as the red line indicates, further verifying the SdH oscillation. The Figure 3c inset shows the dependence of valley position on rotation angle θ, θ is the tilt angle between B and normal direction of sample surface. The plot of valley position of $n = 4.5$ versus tilt angle matches perfectly with fitting curve of $1/\cos(\theta)$ which are strongly expected in two-dimensional (2D) SdH oscillation.

dx.doi.org/10.1021/nl402841x | Nano Lett. 2013, 13, 5344−5349

It is known that SdH oscillation arises from the successive emptying of Landau levels with the increase of the magnetic field. The Landau level N is related to the magnetic field by

$$\frac{1}{B} = \left[\frac{(2\pi e\hbar)}{(S_F)}\right](N + \gamma) \quad (1)$$

where, e is the electron charge, $\hbar$ is the reduced Plank's constant, B is the magnetic flux density, $S_F = \pi k_F^2$ is the extreme cross section of the Fermi surface, k_F is the Fermi wave vector, and $\gamma = 0$ or $1/2$ is the phase factor for regular electrons gas or ideal 2D Dirac fermions, respectively. In principle, γ can be interfered from the Landau level (LL) fan diagram.[32,33] Figure 3d shows the LL fan diagram with the maximum and minimum of MR assigned to Landau level N and $N + 1/2$, respectively, shown in Figure 3d inset. Very good linear fitting gives the intercept of 0.42 and slope F of 3.6 T. That means γ is very close to the 1/2, indicating the existence of Berry's phase of π. As a result, SdH oscillation in SnTe nanowire is caused by the 2D surface Dirac electrons. Considering the Onsager relation $F = (h/4\pi^2 e)S_F$, Fermi wave vector k_F can be estimated to be 1.1×10^6 cm^{-1}. Thus, surface 2D carrier concentration $n_D = k_F^2/4\pi$ is 9.6×10^{10} cm^{-2}. The π Berry phase can be further proved through fitting the plot of resistance fluctuation (ΔR) versus inverse of magnetic field ($1/B$) at 2 K.[34] According to Lifshitz–Kosevich (LK) theory, ΔR is related to $1/B$ by

$$\Delta R = A \exp\left(\frac{-\pi}{\mu B}\right)\cos\left[2\pi\left(\frac{F}{B} + \frac{1}{2} + \gamma\right)\right] \quad (2)$$

where

$$A \propto \frac{\frac{2\pi^2 k_B T}{\hbar\omega_C}}{\sinh\left(\frac{2\pi^2 k_B T}{\hbar\omega_C}\right)} \quad (3)$$

Onsager relation F can be acquired from slope of LL fan diagram. Here, we have not taken account of the amplitude of oscillation $A \exp(-\pi/\mu B)$ since oscillation intensity does not influence the positions of peak and valley. From inset of Figure 3e, we can see peaks and valleys of original data (black square) matches better with the fitting cure of $\gamma = 1/2$ (red circle) than that of $\gamma = 0$ (blue triangle), indicating the quantum oscillation more likely originates from 2D Dirac electrons.

In order to obtain the cyclotron mass (m_c) of SnTe nanowire, temperature-dependent amplitude of SdH oscillation is investigated. The relationship between the oscillation ΔR_{xx} and temperature T satisfy[35]

$$\Delta R_{xx} = \frac{4R_0 e^{-\alpha T_D}\alpha T}{\sinh(\alpha T)} \quad (4)$$

where $\alpha = 2\pi^2 k_B/\hbar\omega_c$, $\omega_c = eB/m_c$ represents the cyclotron frequency, k_B is the Boltzmann's constant, $\hbar$ is the reduced Planck's constant, R_0 is the classical resistance under zero magnetic field, $T_D = \hbar/2\pi k_B\tau$ represents the Dingle temperature, and τ is the total scattering time. m_c can be obtained by fitting the equation $\Delta R_{xx}(T)/\Delta R_{xx}(T_0) = T\sinh(\alpha T_0)/T_0\sinh(\alpha T)(T_0 = 2$ K$)$.[36] As shown in Figure 3e, the best fitting of the temperature-dependent oscillation at $B = 0.72$ T gives $m_c = 0.015\ m_e$, slightly smaller than cyclotron mass of SnTe thin film ($0.07m_e$);[13] m_e denotes the electron rest mass. The cyclotron mass m_c and Fermi velocity ν_F satisfy $m_c\nu_F = \hbar k_F$, thus ν_F can be estimated to be 8.8×10^7 cm s^{-1}, which in turn gives the Fermi level $E_F = m_c\nu_F^2 = 67$ meV, indicating the Fermi level is about 67 meV above the Dirac point for 2D Dirac-like surface state.

To obtain the mean-free path l^{SdH} and the mobility μ_s^{SdH} of surface Dirac electrons, the Dingle temperature T_D is further calculated. Note that $\ln[\Delta R_{xx}\sinh(\alpha T)/4R_0\alpha T]$ is proportional to $1/B$ and T_D can be deduced from the slope of the plot of $\ln[\Delta R_{xx}\sinh(\alpha T)/4R_0\alpha T]$ versus $1/B$ as shown in Figure 3f. Thus T_D and surface state lifetime τ are estimated to be 29 K and 4.2×10^{-14} s, respectively. Then the mean-free path $l^{SdH} = \nu_F\tau$ is 37 nm and the mobility of surface electron $\mu_s^{SdH} = e\tau/m_c$ is 4866 cm^2 V^{-1} s^{-1}.

It is important to emphasize that high-quality single crystalline SnTe nanowire provides the basis of materials for observation of both AB and SdH oscillations. One-dimensional SnTe possesses a large volume to surface ratio that significantly reduces the disturbance from bulk carriers. And the enhanced surface states effect is also expected in SnTe nanowire with decrease of nanowire diameter. Importantly, controllable synthesis technologies developed in this study will promote research of low-dimensional SnTe. Moreover, from the analysis above, we can see both AB and SdH oscillation demonstrate existence of topological surface states in one-dimensional SnTe nanowire. Intriguingly, pronounced AAS effect, which rarely appears in other TIs, is observed in our study. This indicates weak antilocalization effect with strong disorders such as electron diffusion exists in SnTe nanowires. No doubt that our observation will be helpful for future applications of SnTe nanowires in novel spintronics and low-dissipation quantum computation. Parameters of Fermi surface deduced from SdH oscillation in SnTe nanowire as well as in SnTe thin film and Na-doped Bi_2Te_3 nanoplate are listed in Table 1. We can see

Table 1. Comparison of Estimated Surface States Parameters from SdH Oscillation among SnTe Nanowire in This Work, SnTe Thin Film and Na-Doped Bi_2Te_3 Nanoplate

	n_{2D} (10^{10} cm^{-2})	k_F (10^6 cm^{-1})	E_F (meV)	l^{SdH} (nm)	μ_s^{SdH} (cm^{2}V^{-1}S^{1-})
SnTe nanowire	9.6	1.1	67	37	4866
SnTe thin film[13]	30	1.9	40	26	2000
Bi_2Te_3 nanoplate[37]	219	5.24	117	119	3439

that k_F and n_D are comparable to that of SnTe thin film,[13] while the mobility of SnTe nanowire is two times larger than that of SnTe thin film[13] and even larger than that of Na-doped Bi_2Te_3 nanoplates.[38] Generally, materials with high mobility are favorable for high-thermoelectric power and realization of quantum mechanical effect such as the SdH oscillation.[38,39] These important parameters will great benefit further experimental and theoretical study of SnTe nanostructures. It is worth to note that SnTe nanowire synthesized in our work seems to behave slightly different with other TIs. An unusual oscillation phenomenon, angle-dependent period of AB oscillation do not stratify $\Delta B(\theta) = \Delta B(0)/\cos(\theta)$, is observed. We presume this may be because metallic surface only exist on those high-symmetry surface of SnTe, which results in encircling area is not strictly perpendicular to magnetic field direction. Further work needs to be done to address this interesting question. Also, which high-symmetry surface with

dx.doi.org/10.1021/nl402841x | Nano Lett. 2013, 13, 5344–5349

topological states induces SdH effect needs to be elucidated in future work.

In conclusion, we have for the first time synthesized highly single crystalline and pure SnTe nanowires via one-step CVD, which favors the realization of quantum oscillation. Topological crystalline insulator nature of SnTe nanowire has been demonstrated by carrying out AB and SdH oscillation. The discovery of surface Dirac electrons in SnTe nanowire paves the way to its applications in nanoelectronics and spintronics. Valuable parameters on the surface states of SnTe nanowire have also obtained, which will benefit not only the further research of SnTe nanowire but also the exploration of new TCI material.

■ ASSOCIATED CONTENT

Supporting Information

Detail of SnTe nanowires synthesis and characterization, device fabrication, transport measurements, electronic structure of SnTe (001) surface, statistical data of nanowire density and diameter, magnified TEM of SnTe nanowire, AFM images of SnTe nanowires, AB oscillation of SnTe nanowire at 2 and 10 K, plot of MR versus 1/*B*. This material is available free of charge via the Internet at http://pubs.acs.org.

■ AUTHOR INFORMATION

Corresponding Author

*E-mail: hej@nanoctr.cn.

Author Contributions

[†]M.S. and Q.W. contributed equally to the work.

Notes

The authors declare no competing financial interest.

■ ACKNOWLEDGMENTS

This work at National Center for Nanoscience and Technology was supported by the 973 Program of the Ministry of Science and Technology of China (no. 2012CB934103) and the 100-Talents Program of the Chinese Academy of Sciences (no.Y1172911ZX).

■ REFERENCES

(1) Moore, J. E. *Nature* **2010**, *464*, 194−198.
(2) Konig, M.; Wiedmann, S.; Brune, C.; Roth, A.; Buhmann, H.; Molenkamp, L. W.; Qi, X. L.; Zhang, S. C. *Science* **2007**, *318*, 766−770.
(3) Fu, L.; Kane, C. *Phys. Rev. B* **2007**, *76*, 045302.
(4) Qi, X.; Zhang, S. C. *Phys. Today* **2010**, *63*, 33−38.
(5) Fu, L.; Kane, C. *Phys. Rev. Lett.* **2008**, *100*, 096407.
(6) Wang, Q.; Safdar, M.; Wang, Z.; He, J. *Adv. Mater.* **2013**, *25*, 3915−3921.
(7) Chang, C. Z.; Zhang, J.; Feng, X.; Shen, J.; Zhang, Z.; Guo, M.; Li, K.; Ou, Y.; Wei, P.; Wang, L. L.; Ji, Z. Q.; Feng, Y.; Ji, S.; Chen, X.; Jia, J.; Dai, X.; Fang, Z.; Zhang, S. C.; He, K.; Wang, Y.; Lu, L.; Ma, X. C.; Xue, Q. K. *Science* **2013**, *340*, 167−170.
(8) Zhang, H.; Liu, X.; Qi, X.; Dai, X.; Fang, Z.; Zhang, S. *Nat. Phys.* **2009**, *5*, 438−442.
(9) Fu, L. *Phys. Rev. Lett.* **2011**, *106*, 106802.
(10) Hsieh, T. H.; Lin, H.; Liu, J.; Duan, W.; Bansil, A.; Fu, L. *Nat. Commun.* **2012**, *3*, 982.
(11) Xu, S.-Y.; Liu, C.; Alidoust, N.; Neupane, M.; Qian, D.; Belopolski, I.; Denlingerx, J. D.; Wang, Y. J.; Lin, H.; Wray, L. A.; Landolt, G.; Slomski, B.; Dil, J. H.; Marcinkova, A.; Morosan, E.; Gibson, Q.; Sankar, R.; Chou, F. C.; Cava, R. J.; Bansil, A. *Nat. Commun.* **2012**, *3*, 1192.
(12) Tanaka, Y.; Ren, Z.; Sato, T.; Nakayama, K.; Souma, S.; Takahashi, T.; Segawa, K.; Ando, Y. *Nat. Phys.* **2012**, *8*, 800−803.
(13) Taskin, A. A.; Sasaki, S.; Segawa, K.; Ando, Y. arXiv:1305.2470 2013 (accessed June 16, 2013).
(14) Xiu, F.; He, L.; Wang, Y.; Cheng, L.; Chang, L.-T.; Lang, M.; Huang, M.; Kou, X.; Zhou, Y.; Jiang, X.; Chen, Z.; Zou, J.; Shailos, A.; Wang, K. L. *Nat. Nanotechnol.* **2011**, *6*, 216−221.
(15) Peng, P.; Lai, K.; Kong, D.; Meister, S.; Chen, Y.; Qi, X.-L.; Zhang, S.-C.; Shen, Z.-X.; Cui, Y. *Nat. Mater.* **2010**, *9*, 225−229.
(16) Kong, D.; Randel, J. C.; Peng, H.; Cha, J. J.; Meister, S.; Lai, K.; Chen, Y.; Shen, Z. X.; Manoharan, H. C.; Cui, Y. *Nano Lett.* **2010**, *10*, 329−333.
(17) Yan, Y.; Liao, Z.-M.; Zhou, Y.-B.; Wu, H.-C.; Bie, Y.-Q.; Chen, J.-J.; Meng, J.; Wu, X.-S.; Yu, D.-P. *Sci. Rep.* **2013**, *3*, 1264.
(18) Alegria, L. D.; Schroer, M. D.; Chatterjee, A.; Poirier, G. R.; Pretko, M.; Patel, S. K.; Petta, J. R. *Nano Lett.* **2012**, *12*, 4711−4714.
(19) Cho, S.; Kim, D.; Syers, P.; Butch, N. P.; Paglione, J.; Fuhrer, M. S. *Nano Lett.* **2012**, *12*, 469−472.
(20) Kong, D.; Randel, J. C.; Peng, H.; Cha, J. J.; Meister, S.; Lai, K.; Chen, Y.; Shen, Z.; Manoharan, H. C.; Cui, Y. *Nano Lett.* **2010**, *10*, 329−333.
(21) Wang, Y. J.; Tsai, W.; Lin, H.; Xu, S.; Neupane, M.; Hasan, M. Z.; Bansil, A. arXiv:1304.8119v1 2013 (accessed July 15, 2013).
(22) Lee, S. I.; Yoo, J.; Y.Jo, Y.; Park, Y. C.; Kim, H. J.; Koo, H. C.; Kim, J.; Kim, B.; Wang, K. L. *Nano Lett.* **2012**, *12*, 4194−4199.
(23) Bacthtold, A.; Strunk, C.; Salvetat, J. -P.; Bondard, J. -M.; Farro, L.; Nussbaumer, T.; Schonenberger, C. *Nature* **1999**, *397*, 673−675.
(24) Pannetier, B.; Chaussy, J.; Rammal, R.; Gandit, P. *Phys. Rev. B* **1985**, *31*, 3209−3211.
(25) Li, Z.; Qin, Y.; Song, F.; Wang, Q.-H.; Wang, X.; Wang, B.; Ding, H.; Van Haesondonck, C.; Wan, J.; Zhang, Y.; Wang, G. *Appl. Phys. Lett.* **2012**, *100*, 083107.
(26) Bardarson, J. H.; Brouwer, P. W.; Moore, J. E. *Phys. Rev. Lett.* **2010**, *105*, 156803.
(27) Savage, H. T. *Phys. Rev. B* **1972**, *6*, 2292−2304.
(28) Burke, J. R.; Riedl, H. R. *Phys. Rev.* **1969**, *184*, 830−836.
(29) Qu, D. X.; Hor, Y. S.; Xiong, J.; Cava, R. J.; Ong, N. P. *Science* **2010**, *329*, 821−824.
(30) Bao, L.; He, L.; Meyer, N.; Kou, X.; Zhang, P.; Chen, Z. G.; Fedorov, A. V.; Zou, J.; Riedemann, T. M.; Lograsso, T. A.; Wang, K. L.; Tuttle, G.; Xiu, F. *Sci. Rep.* **2012**, *2*, 726.
(31) Cha, J. J.; Kong, D.; Hong, S. S.; Analytis, J. G.; Lai, K.; Cui, Y. *Nano Lett.* **2012**, *12*, 1107−11.
(32) Taskin, A. A.; Ando, Y. *Phys. Rev. B* **2011**, *84*, 035301.
(33) Fang, L.; Jia, Y.; Miller, D. J.; Latimer, M. L.; Xiao, Z. L.; Welp, U.; Crabtree, G. W.; Kwok, W. K. *Nano Lett.* **2012**, *12*, 6164−9.
(34) Tang, H.; Liang, D.; Qiu, R. L. L.; Gao, P. A. X. *ACS Nano* **2011**, *5*, 7510−7516.
(35) Shoenberg, D. *Magnetic Oscillations in Metals*, Cambridge University Press: Cambridge, England, 1984.
(36) Chen, Y. Z.; Bovet, N.; Trier, F.; Christensen, D. V.; Qu, F. M.; Andersen, N. H.; Kasama, T.; Zhang, W.; Giraud, R.; Dufouleur, J.; Jespersen, T. S.; Sun, J. R.; Smith, A.; Nygård, J.; Lu, L.; Büchner, B.; Shen, B. G.; Linderoth, S.; Pryds, N. *Nat.Commun.* **2013**, *4*, 1371.
(37) Wang, Y.; Xiu, F.; Cheng, L.; He, L.; Lang, M.; Tang, J.; Kou, X.; Yu, X.; Jiang, X.; Chen, Z.; Zou, J.; Wang, K. L. *Nano Lett.* **2012**, *12*, 1170−1175.
(38) DiSalvo, F. J. *Science* **1999**, *285*, 703−706.
(39) Beton, P.; Alves, E.; Main, P.; Eaves, L.; Dellow, M.; Henini, M.; Hughes, O.; Beaumont, S.; Wilkinson, C. *Phys. Rev. B* **1990**, *42*, 9229−9232.